

Integration of point-contact microscopy and atomic-force microscopy: Application to characterization of graphite/Pt(111)

M. Enachescu,* D. Schleef,† D. F. Ogletree, and M. Salmeron‡

Materials Sciences Division, Lawrence Berkeley National Laboratory, University of California, Berkeley, California 94720

(Received 24 August 1999)

The electrical current through the point-contact junction of an AFM tip is used to image the surfaces of bulk graphite (HOPG) and the surface of a graphitized carbon monolayer on Pt(111) under ultra-high-vacuum (UHV) conditions. Lattice-resolved images are obtained simultaneously in topography, lateral friction, and contact current channels. Lattice resolution in current maps persisted up to 0.9 mA and pressures of up to 5 GPa. In both bulk graphite and the case of graphitized carbon monolayer on Pt(111), the current images show only one maximum per unit cell. In addition, the contact current images of the graphite monolayer reveal local conductivity variations. We observed local conductivity variations in the form of moiré superstructures resulting from high order commensurability with the Pt lattice. [S0163-1829(99)03248-8]

I. INTRODUCTION

Since the invention of the scanning tunneling microscope (STM),¹ graphite, specifically highly-oriented pyrolytic graphite (HOPG), has become a popular substrate due to its flat cleavage surface and its inert nature, which makes it possible to obtain images in air with “atomic resolution.”^{2,3} However, the literature reports a number of well-known puzzling features, such as uncharacteristically large corrugation amplitudes,^{3–9} enhanced lateral resolution,^{3–10} a weak dependence of the tunneling current on the position of the tip in the direction perpendicular to the surface,¹¹ and anomalously large superperiodicities.¹² These features generated a debate about the imaging mechanism.¹³ In most STM images, one observes only one maximum per unit cell, indicating that the carbon atoms are not imaged as individual units. In a favored explanation, the lattice periodicity is due to the tip imaging a single electron state of the graphite layer.⁶ STM images taken on one monolayer of graphite deposited on metals also show only the lattice periodicity, and not single atomic positions.^{14,15}

In the debate concerning the imaging mechanism of HOPG in STM, it was suggested that the STM tip could be in contact with the HOPG. In order to clarify this issue, Smith *et al.*¹⁶ performed an experiment imaging the HOPG surface by purposely placing the tip in contact with the surface. In contact, the situation is similar to that in point-contact spectroscopy.¹⁷ This mode of microscopy was called point-contact microscopy (PCM),¹⁶ which differs from STM in that the tip is much closer to the sample in the region where the potential barrier is significantly reduced and tip-sample forces are repulsive. In this mode, Smith *et al.* succeeded in imaging the HOPG lattice by measuring the current flowing through the contact. However, they were able to report lattice resolution only at low temperatures, i.e., when the microscope was immersed in liquid helium. Since their contact area involved a large number of atoms, they explained the “atomic” resolution by considering the conduction to be due to a single atom on the tip, which we now consider unlikely. Other experimental evidence indicates that

true tunneling through a vacuum gap might not occur in the case of graphite in normal circumstances, and that the tip is in contact with the surface.¹¹

In AFM contact mode, lattice resolution can be obtained both in topography and friction channels. This is usually explained as the result of stick-slip phenomena.¹⁸ AFM measurements involving a conductive lever have been recently reported^{19–21} in conjunction with tip-sample contact area evaluation. To date, there have been no reports of AFM contact experiments on graphite deposited on metals.

Here we present results on the simultaneous implementation of AFM and PCM techniques by using a conductive AFM lever. We demonstrate the possibility of obtaining lattice resolution concurrently in three channels: topography, friction, and contact current. This is achieved by using both HOPG and 1 ML of graphite deposited on a Pt(111) single-crystal. We show that PCM is as capable of similar lateral resolution as contact AFM imaging. We also found that PCM is sensitive to local conductivity variations due to moiré superstructures resulting from the high order commensurability of the graphite and Pt lattices at different relative rotations. Moreover, we show that lattice resolution in PCM mode is achievable for currents of up to 0.9 mA and contact pressures estimated at 5 GPa.

II. EXPERIMENT

All experiments were performed in a UHV chamber (base pressure 7×10^{-11} Torr) equipped with AFM, Auger electron spectroscopy (AES) and low-energy electron diffraction (LEED).²² Two different samples, HOPG and Pt(111), were used. The HOPG sample was cleaved along the (0001) plane in air and then immediately placed in the vacuum chamber.

The samples could be heated by means of electron bombardment from a hot dispenser cathode. The Pt sample was prepared using standard procedures of Argon-ion bombardment, oxygen treatment, and annealing until a clean and ordered surface was produced, as verified by AES and LEED. The clean surface was then exposed to ethylene at room temperature by backfilling the chamber with ethylene. Exposures were typically greater than 10 Langmuir to ensure saturation

of the Pt(111) surface. After exposure, the sample was heated to about 1250 K, resulting in the decomposition of ethylene and formation of a single monolayer of graphite on the Pt(111) surface. When observed with LEED, we found that the graphite layer produced characteristic fragmented rings,^{23,24} with several dominant bright segments. Some of the ring segments were in-line with the Pt spots, indicating alignment or near-alignment of the graphite and Pt lattices. Others were at an angle relative to the Pt spots, indicating that the graphite lattice was rotated with respect to the Pt lattice.

We measured derivative Auger spectra of the surface with an RFA-type electron analyzer, using a normally incident electron beam with an energy of 2500 eV and retarding field oscillation amplitude of 7 eV peak-to-peak. The ratio of the peak-to-peak heights of the carbon (272 eV) and platinum (237 eV) AES transitions in the derivative spectrum was found to be about 3.8, independent of the amount and method of ethylene exposure. We attribute this to saturation of the surface once a graphite monolayer is formed, such that no further decomposition of ethylene can take place. Because of this, we concluded that there was 1 ML of graphite on the Pt(111) surface. This conclusion is supported by Land *et al.*,^{14,15} who determined by STM, under similar preparation conditions, that the deposited graphite layer was 1-ML thick.

All experiments were performed with a silicon cantilever with a spring constant of 3.5 N/m, and coated with a ~ 20 nm thick conductive tungsten-carbide layer (bulk resistivity $\sim 30 \mu\Omega$ cm).²⁵ The tips were characterized by Scanning Electron Microscopy (SEM) and AES. Previous UHV-AFM measurements on a Pt(111) sample showed that similar tungsten-carbide coated tips are wear resistant and conductive.^{21,26} The tips were treated in UHV immediately prior to the measurements by applying short voltage pulses while in contact and/or by rubbing them at high loads on the surface. We designed and built a flexible I - V converter that allowed us to measure high contact currents by taking measurements spanning the range from pA to mA.

III. RESULTS AND DISCUSSION

A. Topography, friction, and current imaging

Figure 1 shows three $2.5 \text{ nm} \times 2.5 \text{ nm}$ images of the HOPG surface, which were acquired simultaneously. The feedback control was turned off in order to avoid the convolution of topography and friction, and to minimize noise. The images correspond to: (a) normal lever deflection, (b) lateral force or friction, and (c) contact current. A positive bias of 1.0 V was applied to the sample, and the external load during imaging was 100 nN. The average current in (c) was $0.94 \mu\text{A}$, with a modulation of about 17%. In all three images, the 0.246 nm graphite lattice periodicity is clearly observed. Using the DMT contact mechanics model^{27,28} with a measured pull-off force of 115 nN, we estimate that our contact radius is 4.1 nm, and therefore contains about 2000 atoms.²⁹ The contact radius calculated here is only approximate, since the Tabor parameter^{30,31} for this system is 0.67, which indicates that the DMT model is not entirely appropriate. Moreover, none of the analytical contact mechanics models are directly applicable to a non-isotropic material such as graphite.³²

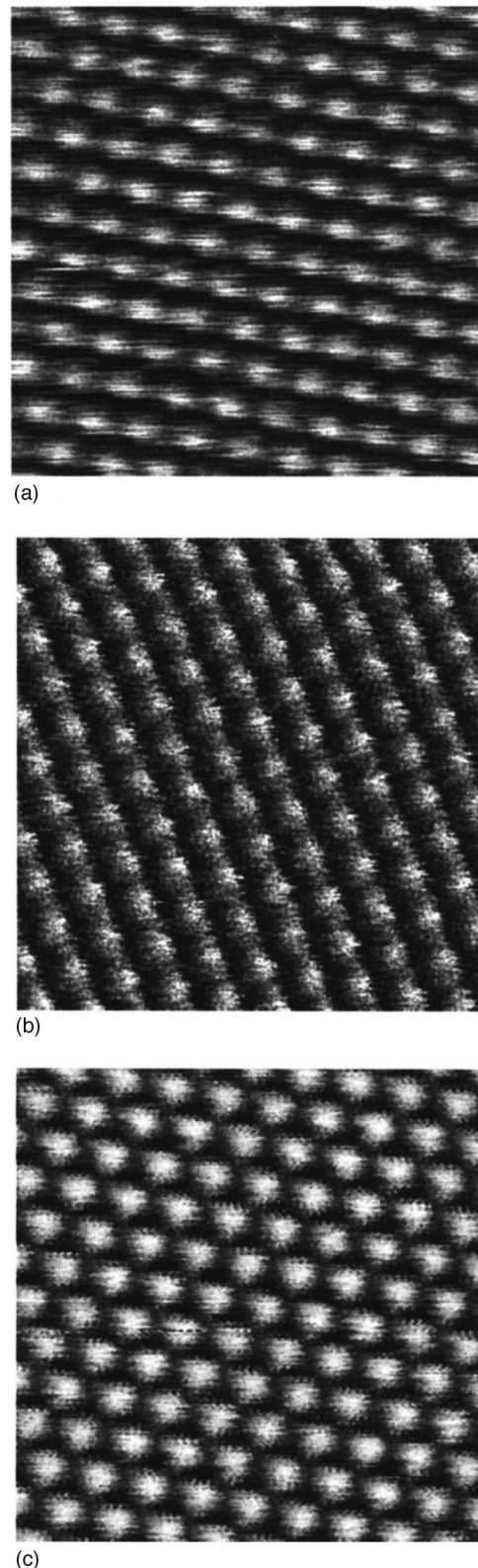


FIG. 1. Simultaneously acquired lattice resolution images of HOPG under UHV conditions: (a) normal lever deflection (with topographical and buckling effects), with a corrugation of 117 pN, corresponding to a height of 33.6 pm; (b) lateral friction image, average force of 0.5 nN and corrugation of 20 nN; (c) PCM image, average current of 945 nA and peak-to-peak corrugation of 160 nA. Image was taken with an applied load of 100 nN without feedback. Image size is $2.5 \text{ nm} \times 2.5 \text{ nm}$.

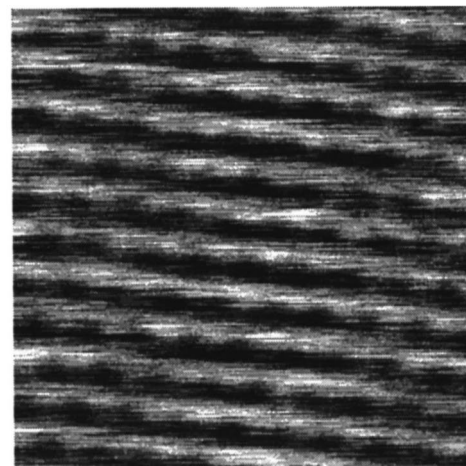
Similar lattice-resolved images were obtained on 1 ML of graphite on Pt(111) [Gr/Pt(111)]. An example of this is shown in Fig. 2. As in the previous case, the $2.5 \text{ nm} \times 2.5 \text{ nm}$ images correspond to: (a) normal lever deflection (under feedback-off conditions), (b) lateral force, and (c) contact current. The external load in this case was 300 nN, and the sample bias was 0.5 V. The average current was $52.7 \mu\text{A}$, with a current modulation of about 2%. In this case, the diameter of the area of contact was similarly estimated to be 5.78 nm, which contains approximately 4000 atoms. Here the 0.246 nm graphite lattice periodicity is also clearly revealed. We were able to obtain lattice resolution at currents up to 0.9 mA and high load. The average pressure at high load was approximately 5 GPa, which is less than the theoretical yield stress of Pt (~ 17 GPa). At pressures higher than 5 GPa and/or currents higher than 0.9 mA, the images were unstable, although the graphite lattice was still visible.

As a side note, we found that we were able to obtain lattice resolution almost all the time and immediately in current mode, while lattice resolution was not as readily visible in the topography and/or friction channels. In many cases, the friction was so low that there was no stick-slip present, i.e., the tip moved continuously over the graphite layer. Because of these reasons, we can rule out the atomic stick-slip mechanism as a reason for the lattice resolution observed in PCM mode.

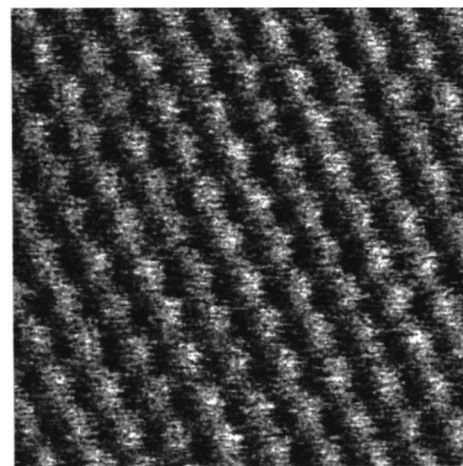
B. Moiré structures

It is known that, for similar preparation conditions,^{14,23,24} graphite forms several orientational domains on a Pt(111) sample. Depending on the preparation conditions and annealing temperature, different sizes and orientations of domains can be prepared. In Fig. 3, we show a $60 \text{ nm} \times 60 \text{ nm}$ image of two graphite domains on Pt(111). The hexagonal periodicity observed in the upper left domain in this image is about 2.0 nm. The large unit cell arises from the superposition of the incommensurate lattices of graphite and Pt(111) at a particular angle. In higher resolution images of this domain, such as the one shown in Fig. 4, the graphite lattice of 0.246 nm, together with the larger 2.0 nm cell, is revealed. Using the real space image and its two-dimensional (2D) Fourier transform, we find that the structure in Fig. 4 corresponds to a superstructure with a $(\sqrt{63} \times \sqrt{63})R19$ unit cell with respect to the graphite lattice. Contrary to standard usage, we report on the moiré structures with respect to the overlayer instead of the substrate, since we can directly count the number of graphite unit cells in the moiré superstructure. Using the known lattice constants of graphite and Pt and the measured angles, we can calculate that the moiré periodicity is almost exactly 7 Pt lattice spacings, and the moiré cell is rotated by 22° with respect to the Pt lattice. Indeed, one can create the 2.0 nm periodic superstructure by rotating the Pt[1 $\bar{1}$ 0] direction with the graphite [$\bar{1}$ 010] direction by 2.68° , as shown in Fig. 5. There is a small lattice misfit of 0.60% associated with the coincidence of the graphite lattice at 1.954 nm and the Pt lattice at 1.942 nm, which can be accounted for by a corresponding relaxation of the graphite layer or the platinum substrate.

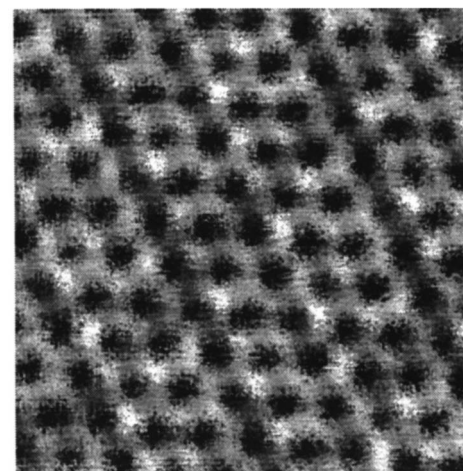
Other graphite domains having different orientations and moiré superstructures have been observed, frequently adja-



(a)



(b)



(c)

FIG. 2. Simultaneously acquired lattice resolution images of 1 ML of graphite deposited on Pt(111) in UHV: (a) normal lever, corrugation of 164 pN; (b) lateral friction image, average force of 0.4 nN and corrugation of 17 nN; (c) PCM image, average current of $53 \mu\text{A}$ and peak-to-peak corrugation of $1.1 \mu\text{A}$ at a bias of 0.53 V. Image was taken with an applied load of 300 nN without feedback. Image size is $2.5 \text{ nm} \times 2.5 \text{ nm}$.

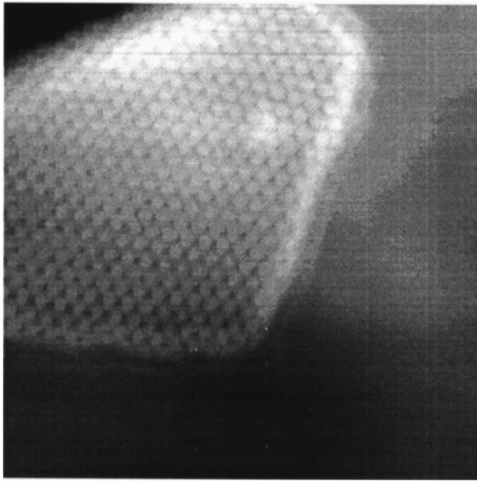


FIG. 3. PCM image showing two moiré superstructure domain on graphite/Pt(111). The upper left has a periodicity of ~ 2.0 nm, and the superstructure lattice was determined to be $(\sqrt{63} \times \sqrt{63})R19$ with respect to the graphite lattice. Image size is $60 \text{ nm} \times 60 \text{ nm}$. The other domain in this image is (5×5) with respect to the graphite lattice, although it is not resolved at this scale.

cent to each other. The image in Fig. 6 shows three contiguous graphite domains, each having different orientations. It is interesting to note that the average current in these domains is different, even if all other conditions (bias, load, tip structure) are the same. The average current can also vary appreciably inside a single domain, such as at a platinum step, as we discuss below.

At higher magnification, different periodic superstructures on each domain can be seen. The image in Fig. 7, which was obtained from the left domain of Fig. 6, shows a (3×3) modulation of the graphite lattice. Its 2D Fourier transform is shown in Fig. 8. The larger hexagonal pattern, marked by six circles, corresponds to the 0.246 nm graphite lattice, while the smaller hexagon, marked by squares, represents the 0.738 nm superstructure lattice. The calculated angle of the graphite lattice with respect to Pt(111) lattice is 19.1° , which is in agreement with the measured angle.

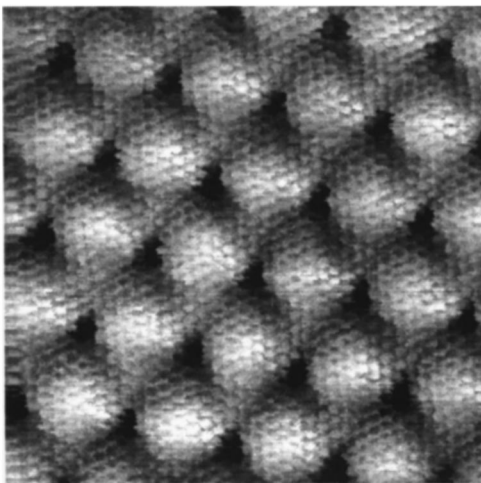


FIG. 4. Close-up image of the $(\sqrt{63} \times \sqrt{63})R19$ domain in Fig. 3, showing the graphite lattice, as well as the moiré superstructure. Image size is $10 \text{ nm} \times 10 \text{ nm}$. Average current is $90 \mu\text{A}$ and corrugation is $5 \mu\text{A}$ at a bias of 0.8 V .

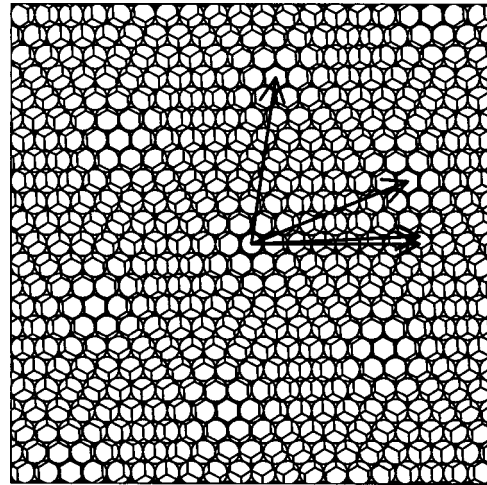


FIG. 5. Schematic of the $(\sqrt{63} \times \sqrt{63})R19$ (with respect to graphite) moiré domain superstructure. With respect to the Pt(111) substrate, the moiré domain is $(7 \times 7)R22$. The Pt atoms are shown as circles with a scaled diameter equal to the lattice constant of Pt (0.278 nm). The graphite lattice is shown as hexagons in which carbon atoms are located at the vertices with C-C distance of 0.142 nm and lattice constant of 0.246 nm . Vectors are drawn to indicate the orientation of the two lattices and the moiré domain. Image size is $5.5 \text{ nm} \times 5.5 \text{ nm}$.

The domain in the middle of Fig. 6 has a (5×5) modulation of the graphite periodicity, as shown in the $5 \text{ nm} \times 5 \text{ nm}$ image of Fig. 9. In this moiré structure, the angle between the graphite and the Pt(111) lattices is calculated to be 23.4° . The domain in the lower right of Fig. 6 was identified as a $(\sqrt{31} \times \sqrt{31})R9$ structure.

Table I is a list of the experimentally observed moiré structures. Using the ratio of the lattice constants of graphite and Pt, we were able to calculate near coincidences of the graphite and Pt lattices at different angles, and thus predict the existence of all of the structures.

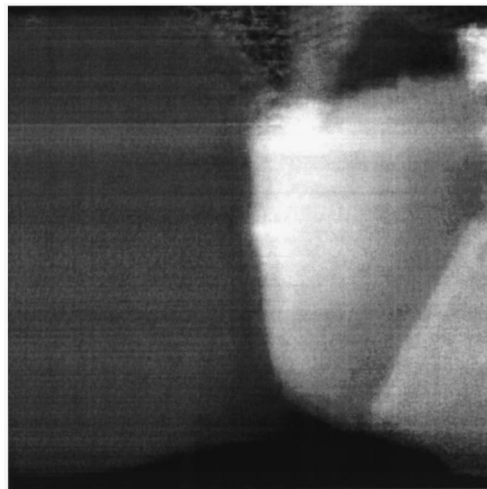


FIG. 6. PCM image showing different moiré domains. Image size is $100 \text{ nm} \times 100 \text{ nm}$. Note that the average current is different on each domain. Average currents are 86 , 100 , and $97 \mu\text{A}$ for the left, center, and right domains, at a bias of 0.8 V .

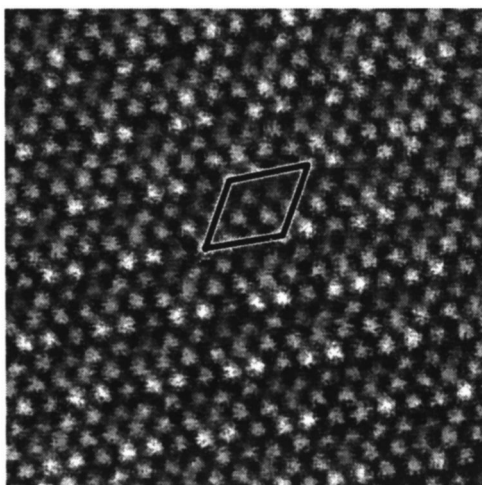


FIG. 7. PCM image of a (3×3) moiré superstructure, showing the graphite lattice. Image size is $5 \text{ nm} \times 5 \text{ nm}$. Average current is $79 \mu\text{A}$ and modulation amplitude is $0.93 \mu\text{A}$ at a bias of 0.7 V .

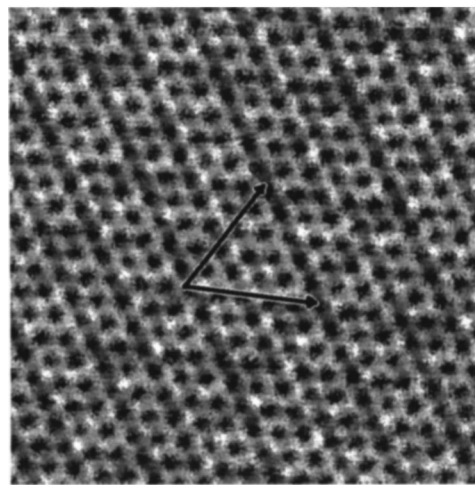


FIG. 9. Close-up image of a (5×5) moiré superstructure, showing the graphite lattice. The arrows indicate the moiré lattice. Image size is $5 \text{ nm} \times 5 \text{ nm}$.

C. Measuring local conductivity using PCM

To determine the lateral resolution of PCM, we acquired images of regions containing platinum steps. We observed that the graphite layer covers the Pt steps continuously from the upper terrace to the lower adjacent one, as shown in Fig. 10. It is important to mention that the image in Fig. 10 is a contact current image. At distances far from the step in this image, the average current is the same on both terraces. However, close to the step, on what we have identified as the lower terrace, the contact current decreases by approximately 30%. At this scale, the topography image shows no contrast, since the graphite layer is almost flat, although tilted with respect to the Pt substrate. On larger scale images of regions containing wide Pt terraces, it is possible to measure a height difference between the terraces. The same (5×5) moiré superstructure was detected on both sides of the Pt step, which indicates that a continuous sheet of graphite is covering the step.

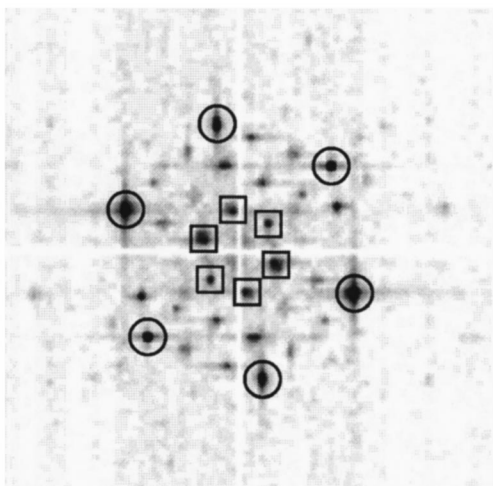


FIG. 8. Fourier transform of image in Fig. 7, showing the graphite lattice periodicity of 0.246 nm marked by circles, and the moiré superstructure periodicity of 0.738 nm marked by squares.

In these experiments, we noticed that the tip-sample contact is not always conductive, unlike in previous experiments with similar cantilevers,²¹ possibly because of contamination as a result of gases used during sample preparation. In particular, when such contamination is observed, current vs. load curves indicate that the current is often not proportional to contact area, with a weak dependence on load, much less than would be expected from contact area variations. The step observed by PCM in Fig. 10 is about 1.5 nm wide, denoting a lateral resolution in PCM mode of this value. Using the DMT contact mechanics model as we did earlier, we estimate that the diameter of the contact area is approximately 8 nm , which indicates a contact AFM lateral resolution of no less than 8 nm . We can use the Sharvin model for point-contact resistance^{33–35} and the measured point-contact resistivity to estimate the area through which current flows in

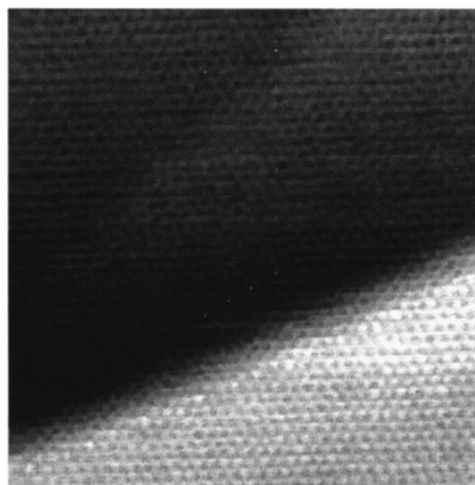


FIG. 10. PCM image of a Pt step covered by a continuous layer of graphite. The topography image (not shown) is completely flat, and does not reveal the presence of a step in the graphite layer at this scale. Image size is $10 \text{ nm} \times 10 \text{ nm}$. The average current is $39 \mu\text{A}$ on the upper terrace and $28 \mu\text{A}$ on the lower terrace at a bias of 1.0 V .

TABLE I. Moiré superstructures experimentally observed in PCM mode. Structures with respect to the Pt lattice are deduced from the measured structures on graphite. In certain cases, the angle of the Pt lattice was known, which aided in the extrapolation.

Moiré periodicity relative to graphite	Moiré periodicity relative to Pt(111)	Angle between graphite and Pt lattices	Moiré periodicity [nm]	Coincidence misfit [%]
(3×3)	$(\sqrt{7} \times \sqrt{7})R19$	19.1	0.738	0.60
$(\sqrt{19} \times \sqrt{19})R23$	(4×4)	23.4	1.07	3.4
(5×5)	$(\sqrt{19} \times \sqrt{19})R23$	23.4	1.23	1.7
$(\sqrt{31} \times \sqrt{31})R9$	(5×5)	8.9	1.37	1.2
$(\sqrt{52} \times \sqrt{52})R14$	$(\sqrt{43} \times \sqrt{43})R8$	21.5, 6.3	1.77	2.5
$(\sqrt{61} \times \sqrt{61})R26$	unknown		1.92	<4.0
$(\sqrt{63} \times \sqrt{63})R19$	$(7 \times 7)R22$	2.7	1.95	0.60
$(\sqrt{73} \times \sqrt{73})R6$	unknown		2.10	<4.9

our contact. The diameter of this area is estimated to be 0.9 nm, which is consistent with the observed lateral resolution in the PCM image.

One explanation for our observation of the different resolutions in AFM and PCM is that the tip is covered with a poorly conducting layer, which is partially broken when the tip is cleaned by applying voltage pulses. This phenomenon may be limited to the tungsten-carbide coating of the tip used in this experiment. Another explanation may be that only the highest-pressure region of the contact area contributes to the point-contact current. However, a graph of current vs. load strongly favors the former explanation. We note that the weak dependence of current on load indicated by these graphs resembles the similarly weak I - Z dependence observed in the past in STM experiments on graphite.¹¹ This supports the idea that, in most cases, STM on graphite is actually point-contact imaging.

The change in local conductivity over the Pt step is likely due to the increased distance between the graphite layer and the underlying Pt substrate. The increased distance acts much like a tunneling barrier. In our measurements, we are able to measure current independently of topography, since the tip-sample contact is affected only by the mechanics of the system. The STM technique uses feedback on current to measure topography, so, for example, in the case of the blanketed Pt step, the STM tip would see the decrease in current and move closer to the sample to compensate. Thus an STM image of a blanketed step would show a topographic step in the graphite layer with a width of 0.2 nm (i.e., typical STM resolution), while contact AFM indicates that the step width is many tens of nanometers. This width is the distance from the platinum step where the graphite layer begins to separate from the platinum substrate. Since the PCM technique is capable of separating mechanical and electrical measurements, it can offer additional insight into the electronic and tribological properties of surfaces.

The STM images of Land *et al.*^{14,15} indicate that there is local conductivity modulation at both the lattice and the moiré periodicities. If we imagine the atoms in our AFM contact contributing to the contact current as a collection of STM tips, one for each atom, the total contact current would be the sum of the contribution of these tips. We would still expect to see both the lattice and the moiré periodicities in

the resulting PCM image, although the magnitude of modulation relative to the average current would decrease. The modulation would sum to zero only in special, destructively interfering cases. This will be discussed in more detail in a future paper.

IV. CONCLUSIONS

We presented the first results of the combination of PCM and AFM techniques, in which current images, obtained on contacts many nanometers in diameter, produced by very high loads (up to 5 GPa), reveal the atomic scale periodicity of the substrate. This surprising observation indicates that, even after averaging over many contact points of atomic dimension, the lattice periodicity does not average out.

We also showed that PCM is capable of measuring variations in local conductivity with a lateral resolution that is similar to the corresponding AFM resolution. Moreover, the technique is capable of separating mechanical and electrical contributions to the measured current. We were able to determine that local conductivity variations arise from different sources, namely, moiré superstructure and the conductivity to the underlying substrate.

We favor point-contact current imaging of lattice resolution as an explanation for many of the STM images on graphite presented in the past, especially in the first decade of STM experiments. In these experiments, it is likely that the tip was in contact with the surface, as in PCM, which explains the weak dependence of “tunneling” current as a function of tip distance.

Point contact current imaging, in conjunction with simultaneous friction and topographic imaging, should be an important tool in current efforts to understand the atomic origin of friction. We are currently applying these techniques to study the tribological behavior of surfaces.

ACKNOWLEDGMENTS

This work was supported by the Director, Office of Science, Office of Basic Energy Sciences, of the U.S. Department of Energy under Contract No. DE-AC03-76SF00098.

- *Permanent address: Department of Physics, University of Bucharest, P.O. Box MG-11, Bucharest, Romania.
- †Also at Department of Physics, University of California, Berkeley, California 94720.
- ‡Author to whom correspondence should be addressed. Electronic address: MBSalmeron@lbl.gov
- ¹G. Binnig, H. Rohrer, C. Gerber, and E. Weibel, *Phys. Rev. Lett.* **50**, 120 (1983).
- ²P. K. Hansma, *Bull. Am. Phys. Soc.* **30**, 251 (1985).
- ³G. Binnig, H. Fuchs, C. Gerber, H. Rohrer, E. Stoll, and E. Tosatti, *Europhys. Lett.* **1**, 31 (1986).
- ⁴A. Selloni, P. Carnevali, E. Tosatti, and C. D. Chen, *Phys. Rev. B* **31**, 2602 (1985).
- ⁵A. Selloni, P. Carnevali, E. Tosatti, and C. D. Chen, *Phys. Rev. B* **34**, 7406 (1986).
- ⁶J. Tersoff, *Phys. Rev. Lett.* **57**, 440 (1986).
- ⁷I. P. Batra and S. Ciraci, *J. Vac. Sci. Technol. A* **6**, 313 (1988).
- ⁸I. P. Batra, N. Garcia, H. Rohrer, H. Salemink, E. Stoll, and S. Ciraci, *Surf. Sci.* **181**, 126 (1987).
- ⁹J. M. Soler, A. M. Baro, N. Garcia, and H. Rohrer, *Phys. Rev. Lett.* **57**, 444 (1986).
- ¹⁰S.-I. Park and C. F. Quate, *Appl. Phys. Lett.* **48**, 112 (1986).
- ¹¹M. Salmeron, D. F. Ogletree, C. Ocal, H. C. Wang, G. Neubauer, W. Kolbe, and G. Meyers, *J. Vac. Sci. Technol. B* **9**, 1347 (1991).
- ¹²M. Kuwabara, D. R. Clarke, and D. A. Smith, *Appl. Phys. Lett.* **56**, 2396 (1990).
- ¹³H. J. Mamin, E. Ganz, D. W. Abraham, R. E. Thomson, and J. Clarke, *Phys. Rev. B* **34**, 9015–18 (1986).
- ¹⁴T. A. Land, T. Michely, R. J. Behm, J. C. Hemminger, and G. Comsa, *Surf. Sci.* **264**, 261 (1992).
- ¹⁵T. A. Land, T. Michely, R. J. Behm, J. C. Hemminger, and G. Comsa, *J. Chem. Phys.* **97**, 6774 (1992).
- ¹⁶D. P. E. Smith, G. Binnig, and C. F. Quate, *Appl. Phys. Lett.* **49**, 1166 (1986).
- ¹⁷I. K. Yanson, I. O. Kulik, and A. G. Batrak, *J. Low Temp. Phys.* **42**, 527 (1981).
- ¹⁸O. Marti, B. Drake, and P. K. Hansma, *Appl. Phys. Lett.* **51**, 484 (1987).
- ¹⁹M. A. Lantz, S. J. O'Shea, and M. E. Welland, *Phys. Rev. B* **56**, 15 345 (1997).
- ²⁰M. A. Lantz, S. J. O'Shea, M. E. Welland, and K. L. Johnson, *Phys. Rev. B* **55**, 10 776 (1997).
- ²¹M. Enachescu, R. J. A. van den Oetelaar, R. W. Carpick, D. F. Ogletree, C. F. J. Flipse, and M. Salmeron, *Phys. Rev. Lett.* **81**, 1877 (1998).
- ²²Q. Dai, R. Vollmer, R. W. Carpick, D. F. Ogletree, and M. Salmeron, *Rev. Sci. Instrum.* **66**, 5266 (1995).
- ²³Z. Hu, D. F. Ogletree, M. A. Van Hove, and G. A. Somorjai, *Surf. Sci.* **180**, 433 (1987).
- ²⁴B. Lang, *Surf. Sci.* **53**, 317 (1975).
- ²⁵NT-MDT Co., Zelenograd Research Institute of Physical Problems, Moscow, Russia.
- ²⁶M. Enachescu, R. W. Carpick, D. F. Ogletree, and M. Salmeron (unpublished).
- ²⁷V. M. Muller, B. V. Derjaguin, and Y. P. Toporov, *Colloids Surface* **7**, 251 (1983).
- ²⁸B. V. Derjaguin, V. M. Muller, and Y. P. Toporov, *J. Colloid Interface Sci.* **53**, 314 (1975).
- ²⁹Elastic moduli and Poisson ratios used in calculations are: Pt, $E = 168$ GPa, $\nu = 0.38$; tungsten carbide, $E = 714$ GPa, $\nu = 0.22$; and HOPG, $E = 36.5$ GPa, $\nu = 0.25$. The elastic modulus for HOPG is the modulus along the [0001] direction. The tip radius, as measured with a faceted SrTiO₃ reference sample, is 100 nm. See G. W. C. Kaye, *Tables of Physical and Chemical Constants, and Some Mathematical Functions* (Longmans, London, 1966), 13th ed., B. T. Kelly, *Physics of Graphite* (Applied Science Publishers, London, 1981); M. M. Schwartz, *Ceramic Joining* (ASM International, Materials Park, Ohio, 1990).
- ³⁰J. A. Greenwood and K. L. Johnson, *J. Phys. D* **31**, 3279 (1998).
- ³¹D. Tabor, *J. Colloid Interface Sci.* **58**, 2 (1977).
- ³²I. Sridhar, K. L. Johnson, and N. A. Fleck, *J. Phys. D* **30**, 1710 (1997).
- ³³Y. V. Sharvin, *Zh. Eksp. Teor. Fiz.* **48**, 984 (1965) [*Sov. Phys. JETP* **21**, 655 (1965)].
- ³⁴G. Wexler, *Proc. Phys. Soc. London* **89**, 927 (1966).
- ³⁵Contact resistance is calculated in the Sharvin model by the equation $R = (4\rho l)/(3\pi r^2)$, where ρ is the bulk resistivity, l is the mean free path, and r is the radius of the contact.